CORA Cork Open Research Archive
Cartlann Taighde Oscailte Chorcaí

Title	Reactivity of metal oxide nanocluster modified rutile and anatase TiO2: Oxygen vacancy formation and CO2 interaction
Authors	Fronzi, Marco;Daly, William;Nolan, Michael
Publication date	2015-12-02
Original Citation	Fronzi, M., Daly, W. and Nolan, M. (2016) 'Reactivity of metal oxide nanocluster modified rutile and anatase TiO2: Oxygen vacancy formation and CO2 interaction', Applied Catalysis A: General, 521(Supplement C), pp. 240-249. doi: 10.1016/j.apcata.2015.11.038
Type of publication	Article (peer-reviewed)
Link to publisher's version	http://www.sciencedirect.com/science/article/pii/S0926860X15302659 - 10.1016/j.apcata.2015.11.038
Rights	© 2015 Elsevier B.V. This manuscript version is made available under the CC BY-NC-ND 4.0 license.5 - http://creativecommons.org/licenses/by-nc-nd/4.0/
Download date	2026-11-06 09:43:38
Item downloaded from	https://hdl.handle.net/10468/4940

UCC
University College Cork, Ireland
Coláiste na hOllscoile Corcaigh

Reactivity of Metal Oxide Nanocluster Modified Rutile and Anatase TiO_2: Oxygen Vacancy Formation and CO_2 Interaction

Marco Fronzi,* William Daly, and Michael Nolan†

Tyndall National Institute, Lee Maltings, University College Cork, Cork, Ireland

The reduction of CO_2 to fuels is an active research topic with much interest in using solar radiation and photocatalysts to transform CO_2 into higher value chemicals. However, to date there are no photocatalysts known that can use solar radiation to efficiently reduce CO_2. One particularly difficult problem is activating CO_2 due to its high stability. In this paper we use density functional theory simulations to study novel surface modified TiO_2 composites, based on modifying rutile and anatase TiO_2 with molecular-sized metal oxide nanoclusters of SnO, ZrO_2 and CeO_2 and the interaction between CO_2 and nanocluster-modified TiO_2. We show that reduction of the supported nanocluster is favourable which then provides reduced cations and sites for CO_2 adsorption. The atomic structures and energies of different adsorption configurations of CO_2 on the reduced modified TiO_2 composites are studied. Generally on reduced SnO and CeO_2 nanoclusters, the interaction of CO_2 is weak producing adsorbed carbonates. On reduced ZrO_2, we find a stronger interaction with CO_2 and carbonate formation. The role of the energies of oxygen vacancy formation in CO_2 adsorption is important because if reduction is too favourable, the interaction with CO_2 is not so favourable. We do find an adsorption configuration of CO_2 at reduced CeO_2 where a C-O bond breaks, releasing CO and filling the oxygen vacancy site in the supported ceria nanocluster. These initial results for the interaction of CO_2 at surface modified TiO_2 provide important insights for future work on CO_2 reduction using novel materials.

keywords: Photocatalysis, TiO_2, Surface Modification, Density Functional Theory, Oxygen Vacancy, CO_2, Adsorption

I. INTRODUCTION

The growing global demands for energy and the depletion of fossil fuel resources are motivating scientific research to find alternative, sustainable and renewable sources of energy [1, 2]. The exploitation of energy from solar light, by photo-voltaic and photo-catalyst cells, has emerged as one of the most promising viable routes for the near future. The strength of solar to electro-chemical energy

*Corresponding author

E-mail: marco.fronzi@tyndall.ie

†Corresponding author

E-mail: michael.nolan@tyndall.ie

conversion is that the energy produced can be stored in chemical bonds and used when needed, which is an evident advantage in practical use of solar energy, mitigating against the variability in solar irradiation.

Photocatalysis [3–5] will be an important technology in exploiting solar energy for fuel production. Key applications of photocatalytic mechanisms are found in those systems that convert sunlight, water, and carbon dioxide into hydrocarbons; this then represents a clean energy technology, with no emission of greenhouse gases during fuel production, and a sustainable carrier of solar energy.

The main component of a typical photocatalyst device is a photo-sensitive semiconducting material where photo-induced molecular transformations and reactions take place. At the catalyst surface, low energy and usually simple molecules are converted into high energy compounds, where the new chemical bonds play the role of energy storage. Given the pressing societal issues of fossil fuel supply squeezes and greenhouse gas emissions, a particularly important process is represented by the conversion of CO_2, emitted from burning fossil fuels, into complex carbon fuels, including CH_4, CH_3OH, HCOOH etc. [6–10] This has the advantage that waste CO_2 can be captured and exposed to water and sunlight over a photocatalyst and transformed into fuels with reasonable efficiency (although to date, the efficiencies of CO_2 reduction have been small [7]).

Titanium dioxide (TiO_2), represents one of the most suitable materials for solar to chemical energy conversion [11–13]. This is due to its photosensitive surfaces combined with good chemical stability in different solutions, low cost, abundance and ease of processing. Rutile and anatase are the dominant phases of TiO_2 and the rutile (110) and anatase (101) surfaces show the generation of photo-currents under solar light exposure and a sufficiently long electron-hole lifetime to be useful as a practical photocatalyst [14, 15].

The two primary differences between the two phases of TiO_2 that give them their distinct characteristics are the slightly different band gap energy (about 3.0 eV in rutile versus 3.2 eV in anatase [11]) and the different electron-hole recombination time, which is larger in anatase [16], so that anatase is considered a more active photocatalyst; however, anatase transforms into rutile at sufficiently higher temperatures [17, 18] Both phases show a large band gap that allows the absorption of light in the ultra violet range, which represents only ($\sim$4%) of the total solar flux. Therefore, any reduction of the band gap energy would correspond to an increase of light harvesting capability and this will improve the efficiency of the device under solar irradiation.[3–5, 19]

Several ways have been explored to overcome this major issue, from metal and non-metal doping, [3–5, 19] to surface sensitising through dyes, [20–22] or with semiconductor quantum dots [23–25]. In recent years, metal oxide nanocluster (NC) modification of TiO_2 surfaces and films has been shown to be a successful approach to modify the light absorption characteristics of TiO_2 and enhance its

photocatalytic activity, at least for oxidation reactions. [12, 26–29]

One of the most important properties of NCs is that the band energies are controlled by size quantization and in the sub-nm regime, the properties of the NC depend on its composition. When the NC modifier is adsorbed onto the surface of a photosensitive material, such as TiO_2, the modifier can change the band gap (or absorption edge) by either modifying the width of the host valence or conduction band edges, or by creating new states inside the previous band gap. This will therefore modify the light absorption properties of TiO_2 and can induce a shift towards visible light absorption. While light absorption in the visible region is obviously desirable for visible light activated photocatalysts, it is not sufficient to produce a photocatalyst that is more active than TiO_2, as the fate of the photogenerated electrons and holes is important. Doping of TiO_2 can reduce photocatalytic activity as the defect states introduced by doping can enhance charge recombination and thus lower the activity. By contrast, NC modification of TiO_2 plays a crucial role in inhibiting charge recombination, as proposed in our previous density functional theory (DFT) studies of NC-modified TiO_2 [30–32] and in photoluminesence (PL) experiments.[28, 29] A reduction in the well known PL emission feature of TiO_2 at 520 nm is found upon modification with oxide nanoclusters [28, 29] and this correlates with the enhanced photocatalytic activity of NC-modified TiO_2. The origin of this result is that the NC-modification, which modifies the valence band edge [29], results in spatial separation of photogenerated electrons (on the TiO_2 surface) and holes (in the nanocluster modifier). This reduces the recombination of charge carriers and increases the reactivity towards molecules compared to unmodified TiO_2. In addition, due to the low coordination numbers of metal and oxygen sites, with 3-fold and 4-fold metal and singly coordinated oxygen sites available, [30] the metal oxide nanoclusters offer active sites for adsorption of molecules when compared with extended surfaces.

Our previous modelling and experimental studies show how a large class of metal oxide nanocluster modifiers on TiO_2 may offer increased visible light absorption, together with excellent chemical reactivity [29]. Therefore, the exploitation of TiO_2 surface modification represents an efficient, low cost and environmentally friendly solution in developing photoactive materials for energy conversion. The previous work on these composite photocatalysts [29, 30, 33–36] has focussed on understanding how visible light activity can be induced through surface modification (simulation and experiment) and studying the activity for oxidation reactions (experiment). However, the role of the NC-modification in the catalytic activity of the composite photocatalyst has not been explored in detail. In addition, since the chemistry of metal oxide surfaces is determined by the presence of point defects such as oxygen vacancies, the interplay between the defects, the adsorbed NCs and the molecules of interest, such as H_2O or CO_2 is crucial to understand the catalytic activity of these composite photocatalysts, which is, however, not yet completely clear [37, 38]. In view of this, a detailed analysis of NC modified

TiO_2 surfaces and their interaction with molecules and the role of oxygen vacancies is crucial in the development of this novel class of photo-active materials. Since the activity of a visible light activate photocatalyst depends on light absorption, charge separation and the reaction of target molecules with the catalyst, the present study is concerned with each of the above points in connection with photo-catalytic CO_2 reduction, in particular the last point on the initial interaction and possible activation of CO_2 at the photocatalyst.

In this paper, we present a DFT study of metal oxide NC modified TiO_2 with a focus on the reactivity of NC modified TiO_2 anatase (101) and rutile (110) surfaces and their potential for CO_2 reduction. The metal oxide NC modifiers are CeO_2, SnO, and ZrO_2, covering a range of metal oxides with different reducibility and energy gaps. The key work in this paper is the analysis of the formation of oxygen vacancies on these composite structures and the analysis of the interaction of the modified surfaces with CO_2 in presence of the oxygen vacancies. This will allow us to obtain the first insights into the ability of the NC-modified TiO_2 composites to (1) support oxygen vacancies and (2) activate CO_2, so that it may be reduced. The results of this paper thus provide the first insights into activation of CO_2 with metal oxide NC modified TiO_2 composite photocatalysts.

II. COMPUTATIONAL METHODS

The calculations presented in this work are performed within a Density Functional Theory approach, using the Generalized Gradient Approximation (GGA) from Perdew-Burke-Ernzerhof (PBE) [39] for the exchange-correlation term. We use periodic boundary conditions with a plane wave basis set, implemented in the VASP code [40, 41]. The cut-off energy for the valence electrons is 400 eV. The core-valence interaction is described by the projector augmented wave method [42], with 4 valence electrons for Ti, 6 for O, 4 for Sn, 12 for Ce, 4 for Zr, 4 for C and 1 for H species. Γ point sampling has been used for the (2×4) expansion of rutile (110) and anatase (101) surfaces. The computed lattice constants of the rutile and anatase bulk are $a = b = 4.69$ Å and $c = 3.04$ Å, and $a = b = 3.90$ Å and $c = 9.72$ Å, respectively. The surface slabs consist of 18 and 12 mono-layers for the rutile (110) and anatase (101) surfaces, respectively, with a vacuum gap of 20 Å, while the dimensions of the nanocluster used give a coverage of approximatively 1/4 ML on both rutile (110) and anatase (101) surfaces.

The nanoclusters are adsorbed on the TiO_2 surfaces in different adsorption configurations and then allowed to relax with no constraints on symmetry or atomic positions. For these calculations, the initial TiO_2 surfaces are perfect model surfaces, with no point defects or surface hydroxyl groups which are generally present on real TiO_2 surface; work on these aspects of nanocluster modified TiO_2 is ongoing.

The convergence criteria for the energy and forces are 10^{-5} eV and 10^{-2} eV/Å^2, respectively.

In order to correctly describe the partially occupied states of Ti_{3d}, O_{2p}, and Ce_{4f}, a Hubbard correction for the exchange-correlation potential has been employed. The partially occupied states are described with U(Ti)=4.5 eV, U(Ce)=5.0 eV and U(O)=5.5 eV values, all of which have been used in our previous works [30–32, 43].

While the Hubbard +U correction is widely used for Ti and Ce as it gives a consistent description of reduced and oxidised electronic states and the associated local geometry, previous work found that this correction can also be required when describing partially filled O_{2p} states that can result after valence band hole formation[44, 45] which is important when we analyse the photoexcited state of these composite materials [30–32]; while calculations of the photoexcited state with adsorbates are the subject of ongoing work, we use the +U correction on the O 2p states in this paper to ensure consistency throughout all calculations. Although the +U correction can give a small increase in the TiO_2 energy gap, it still underestimates the magnitude of the energy gap. However, applying, e.g. a Hybrid DFT approach, that generally obtains a consistent band gap, for these composite systems (with over 300 atoms) within a plane wave basis set is not possible at present.

III. RESULTS

A. The Properties of Metal Oxide Nanocluster Modifier TiO_2 and Formation of Oxygen Vacancies

We first analyse nanocluster adsorption energies and geometries on stoichiometric rutile and anatase TiO_2 surfaces. Relaxed atomic configurations of NC-modified TiO_2 with MC compositions Sn_4O_4, Zr_3O_6 and Ce_3O_5 are shown in Figure 1; the exception is for the CeO_2 NC which has been adsorbed only on rutile (110). The NCs considered in this section are in their stoichiometric form, while the CeO_2 NC is present with composition Ce_3O_5, that is, in its reduced form, due our finding that in the adsorbed Ce_3O_6 NC an oxygen vacancy is formed spontaneously at T = 0 K. This is consistent with findings from work on small CeO_2 NC in which reduced Ce^{3+} is present [46].

The choice of these specific nanocluster compositions comes from our previous work on metal oxide NC modified TiO_2 [30–32, 47] where we have shown that these are reasonable models of oxide NC modified TiO_2, which can be studied at a reasonable computational cost. Although there are many possible adsorption structures of oxide NCs on the TiO_2 surfaces, with a range of adsorption energies, e.g. [47, 48], we find that once the nanoclusters are adsorbed in stable configurations, the trends in key properties, such as band gap reduction are unaffected. For this paper, we aim to use representative

NC-modified TiO_2 composites to examine the potentials of these structures in modifying the electronic structure and CO_2 activation of TiO_2.

The NC adsorption energies on the TiO_2 surfaces have been calculated as follows:

$$E_{\mathrm{Ads}} = E_{\mathrm{Surf+A}} - E_{\mathrm{Surf}} - E_A \quad , \tag{1}$$

where $E_{\mathrm{Surf+A}}$, E_{Surf} and E_{A} are the energies of the adsorbate(NC)-surface system, the unmodified TiO_2 surface and the gas phase NC, respectively.

The calculated adsorption energies are shown in Table I and the relaxed adsorption structures are shown in Fig. 1. The negative energies in each case show a favourable interaction between the nanocluster and the TiO_2 surfaces and the large adsorption energies between -4.09 and -8.83 eV show that the interaction between the Nanocluster and TiO_2 is very strong. This means that the nanocluster will be expected to remain stable on the surface (that is, it will not desorb) and furthermore the nanoclusters will not migrate over the surface to form larger aggregates as shown in Ref. [47].

After relaxation of nanocluster-modified TiO_2, new nanocluster to surface bonds are formed; these are between surface Ti and nanocluster oxygen and nanocluster cations and TiO_2 surface oxygen. In general, the more new surface-to-nanocluster bonds formed the more stable is the resulting nanocluster-surface composite [47, 48].

An interesting feature of these structures is that after relaxation the rutile (110) surafce is generally not significantly perturbed, apart from a downwards migration of an originally 5-fold coordinated surface Ti atom that is now bonded with oxygen from the nanocluster; this Ti atom migrates towards the next sublayer by ca. 0.1 Å upon binding with oxygen from the nanocluster.

The local atomic structure around the nanocluster adsorption site is modified and the typical change of the Ti-O bond lengths at the surface is as large as 7% on anatase (101) and 8% on rutile (110); the surface Ti−O bond-length in the unmodified surfaces are 1.87, 1.95 and 2.01 Å in rutile (110) and 1.89, 2.06, 2.14, 1.99 and 1.92 Å in anatase (101), indicating a clear distortion of the lattice at the interface. In particular for anatase (101), there is always at least one surface oxygen atom that migrates off its lattice site to bind with the adsorbed nanocluster, which we have also observed on anatase (001) modified with different nanoclusters [35, 49, 50]

Figure 2 shows the electronic density of states (PEDOS) projected onto O 2p states in the nanocluster and TiO_2 surface, Ti 3d states, Sn 5s/5p states, Zr 4d states and Ce 4f states for the different NC-modified TiO_2 composites. For the p-block oxide SnO, on both rutile and anatase, there are SnO Sn 5s and O 2p derived electronic states present in the previously empty TiO_2 valence to conduction band energy gap. This has the effect of reducing the energy gap between the occupied and empty

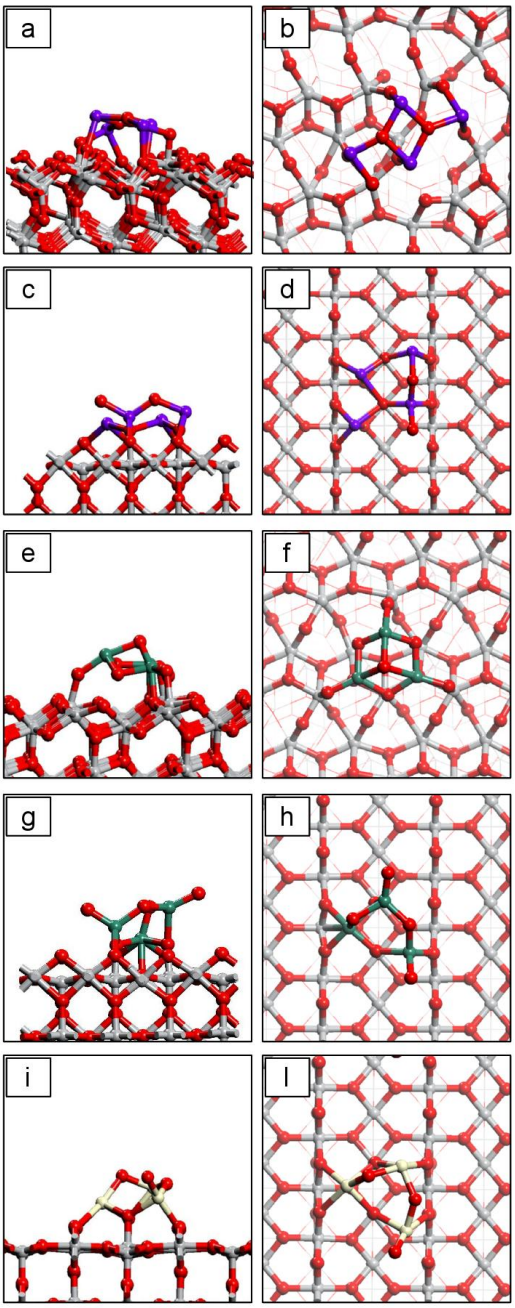


Figure 1: (Color online) Atomic structure of Sn_4O_4, Zr_3O_6 and Ce_3O_5 nanoclusters adsorbed on anatase (101) and rutile (110) TiO_2 surfaces. The left panels show a side view and the right panels a top view. a) and b) represent Sn_4O_4 on anatase (101), c) and d) represent Sn_4O_4 on rutile (110), e) and f) represent Zr_3O_6 on anatase (101), g) and h) represent Zr_3O_6 on rutile (110) and i) and l) represent Ce_3O_5 on rutile (110). Light gray and red spheres represent titanium and oxygen atoms, while violet, green and white sphere represent tin, zirconium and cerium atoms, respectively

states which shifts light absorption into the visible region; a full description of this system is given in Ref. [49].

For Zr_3O_6 modified rutile and anatase, there are new ZrO_2 derived states in the previously empty TiO_2 band gap, which are dominated by occupied O 2p states from ZrO_2. These lie quite high in the

Table I: Computed adsorption energies (in eV) of metal oxide nanoclusters adsorbed on anatase (101) and rutile (110) TiO_2 surfaces.

Nanocluster-TiO_2 Surface	Adsorption Energy (eV)
Sn_4O_4-anatase(101)	−6.37
Sn_4O_4-rutile(110)	−4.09
Zr_3O_6-anatase(101)	−8.83
Zr_3O_6-rutile(110)	−5.40
Ce_3O_5-rutile(110)	−6.30

TiO_2 band gap, suggesting a significant red shift in light absorption, particularly for ZrO_2-modified anatase.

Finally, for Ce_3O_5-modified rutile (110), the PEODS in figure 2(e) shows the formation of reduced Ce^{3+} cations, as evidenced by the occupied Ce 4f states that are present after oxygen vacancy formation - these states lie between the top of the valence band and the empty Ce 4f states [43, 51].

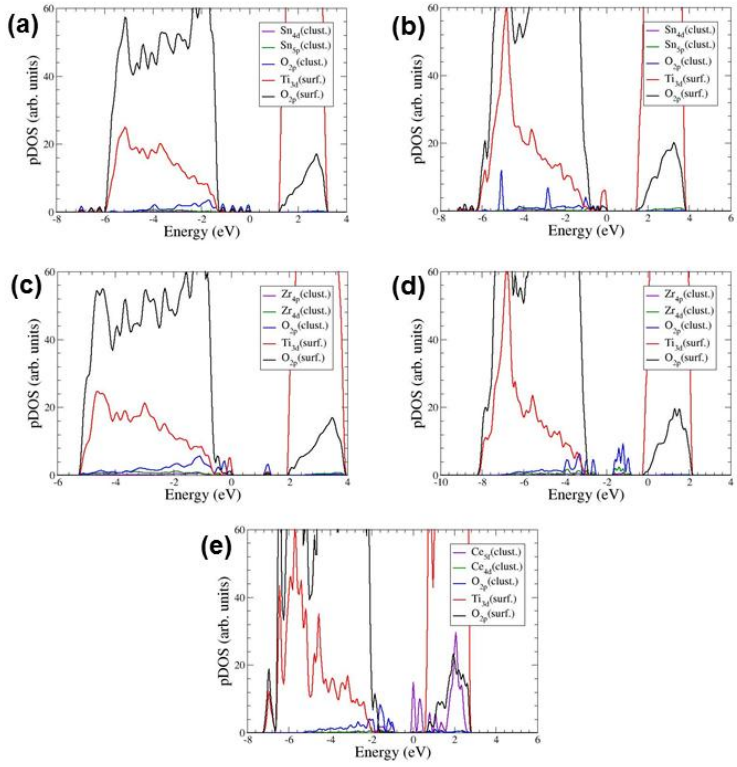


Figure 2: (Color online) Projected electronic density of states onto O 2p states in the nanocluster and TiO_2 surface, Ti 3d states, Sn 5s/5p states, Zr 4d states and Ce 4f states for: a): Sn_4O_4 on anatase (101), b) Sn_4O_4 on rutile (110), c) Zr_3O_6 on anatase (101), d) Zr_3O_6 on rutile (110) and e) Ce_3O_5 on rutile (110).

Starting from the relaxed composite structures, shown in Figure 1, we have removed each oxygen

in the Nanocluster modifier and computed the vacancy formation energies as follows:

$$E_{\mathrm{V_O}} = E_{\mathrm{Surf+V_O}} - E_{\mathrm{Surf}} - \frac{1}{2}E_{\mathrm{O_2}} \quad , \tag{2}$$

where $E_{\mathrm{Surf+V_O}}$, E_{Surf} and $E_{\mathrm{O_2}}$ are the energies of the slab after the introduction of a vacancy, the energy of the stoichiometric slab and the energy of free oxygen in gas phase, respectively. blue The oxygen atoms removed from the nanocluster are labelled with Roman numerals in Figure 3.

Upon examining the energies of the oxygen vacancy sites, it is interesting that the energies suggest spontaneous oxygen vacancy formation at 0K for the Sn_4O_4 nanocluster on the rutile (110) surface; the magnitude of this energy indicates that an Sn_4O_3 nanocluster will be present on this surface. For the Sn_4O_4 NC supported on anatase (101), the lowest oxygen vacancy formation energy is 0.13 eV, which suggests the oxygen can be removed at low temperatures.

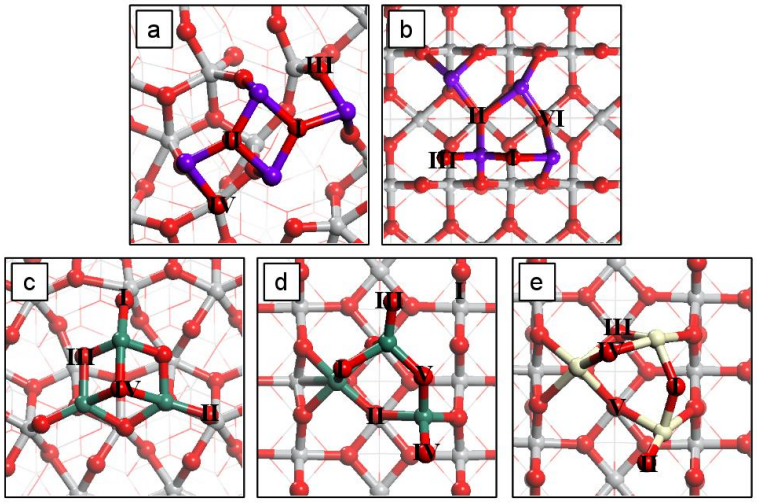


Figure 3: (Color online) Top view of the atomic structure of a) Sn_4O_4 on anatase (101), b) Sn_4O_4 on rutile (110), c) Zr_3O_6 on anatase (101), d) Zr_3O_6 on rutile (110) and e) Ce_3O_5 on rutile (110) TiO_2 surfaces, in which the Latin numbers indicate the position of the oxygen atoms corresponding to the vacancy formation energies reported in Tab. II. Light gray and red spheres represent titanium and oxygen atoms, while violet, green and white sphere represent tin, zirconium and cerium atoms, respectively

For the remaining surface modified composite structures, the computed oxygen vacancy formation energies are positive, Table 2. The most stable O vacancy structure for ZrO_2 has a cost of only 0.56 eV on anatase and 0.48 eV on rutile. For the pre-reduced CeO_2 nanocluster, the cost to form the next oxygen vacancy is only 0.31 eV. These relatively low vacancy formation energies indicate that these composite structures will be quite reactive and it is interesting to note that the magnitude of the vacancy formation energies are significantly lower than in the corresponding bulk oxides, which are around 1.3 eV for the neutral oxygen vacancy under oxygen rich conditions in bulk SnO [52] close to 9 eV for bulk ZrO_2 [53] and 4.5 eV for bulk CeO_2 [54]. Thus the nanostructure of the metal oxide

nanocluster modifier induces a higher degree of reactivity compared to its bulk structure, at least as measured by the oxygen vacancy formation energy.

Table II: Computed oxygen vacancy formation energies, in eV, in Sn_4O_4, Zr_3O_6 and Ce_3O_5 nanocluster modified anatase (101) and rutile (110) TiO_2 surfaces. Latin numbers indicate the position of the oxygen removed from the cluster as depicted in Fig. 3.

Oxygen Vacancy Structure	Formation Energy (eV)
Anatase (101)-Sn_4O_4-V_O-I	2.65
Anatase (101)-Sn_4O_4-V_O-II	1.11
Anatase (101)-Sn_4O_4-V_O-III	0.13
Anatase (101)-Sn_4O_4-V_O-IV	0.99
Rutile (101)-Sn_4O_4-V_O-I	−1.03
Rutile (101)-Sn_4O_4-V_O-II	2.62
Rutile (101)-Sn_4O_4-V_O-III	1.50
Rutile (101)-Sn_4O_4-V_O-IV	2.52
Anatase (101)-Zr_3O_6-V_O-I	2.57
Anatase (101)-Zr_3O_6-V_O-II	1.11
Anatase (101)-Zr_3O_6-V_O-III	1.07
Anatase (101)-Zr_3O_6-V_O-IV	0.56
Rutile (101)-Zr_3O_6-V_O-I	0.70
Rutile (101)-Zr_3O_6-V_O-II	3.74
Rutile (101)-Zr_3O_6-V_O-III	0.48
Rutile (101)-Zr_3O_6-V_O-IV	0.48
Rutile (101)-Zr_3O_6-V_O-V	2.92
Rutile (101)-Ce_3O_5-V_O-I	1.08
Rutile (101)-Ce_3O_5-V_O-II	1.06
Rutile (101)-Ce_3O_5-V_O-III	1.14
Rutile (101)-Ce_3O_5-V_O-IV	0.31
Rutile (101)-Ce_3O_5-V_O-V	1.39

After vacancy formation, we observe further geometry distortions in the nanocluster structures, see figure 4. The typical Sn-O distance in the Sn_4O_3 clusters (after O vacancy formation) is between 1.91 and 2.10 Å. In Zr_3O_5-modified rutile the Zr-O distances are 1.81-2.19 Å and for Zr_3O_5-modified anatase, Zr-O distances are 1.97-2.17 Å. Finally, in Ce_3O_5 the Ce-O distances are 1.85 and 2.40 Å. When the oxygen vacancy is formed, there is an increase in the metal to oxygen distance of up to 7%, indicating an evident structural distortion of the nanoclusters, which may potentially favour molecular adsorption.

In figure 4 we also show the computed excess spin density for the surface modified TiO_2 composite studied after formation of the most stable oxygen vacancy structure. The spin density plot shows where the two electrons released upon formation of a neutral oxygen vacancy will be located after relaxation (a triplet electronic state is used in these calculations to enable the spin density to be determined; the energies of the triplet and singlet spin configurations tend to be rather close in these oxides with O vacancies, e.g. [55]). This analysis allows us to examine trends in electron localizations in the reduced composite structures, allowing the reducibility of the nanocluster compared to TiO_2 to be assessed.

The spin density plots in figure 4 show that for Zr_3O_5-modified anatase and rutile and Sn_4O_4-modified anatase and rutile composites, two reduced Ti^{3+} cations are formed at the surface upon transfer of two electrons to the oxide. By contrast, in Ce_3O_4-modified rutile, electron localization occurs at two Ce atoms in the nanocluster, with no reduction of Ti atoms in the surface. The spin density results are further supported by a Bader analysis of the net atomic charges. The typical net atomic charges on Ti^{4+} and Ce^{4+} species are around 1.25 and 9.5 electrons. After formation of the oxygen vacancy on the SnO and ZrO_2 nanocluster-modified surfaces, there are two Ti sites in the surface with net charges of 1.7 electrons, which is typical for the formation of reduced Ti^{3+} species (while all other Ti cations show net charges around 1.25 electrons). In the CeO_2 modified rutile structure, the Ce atom sites which carry the spin density have net atomic charges of 9.95 and 9.88 electrons. Thus, the Bader charges confirm the reduction of Ti in the TiO_2 surface after vacancy formation if the nanocluster modifier is non-reducible but reduction of Ce in the CeO_2 nanocluster modifier and with no Ti reduction.

The projected electronic density of states for the oxygen vacancies described above are shown in Fig. 5. The main feature of the PEDOS in this case is that as well as the presence of electronic states from the NC modifiers, there are new electronic states in the TiO_2 band gap that arise from the formation of reduced Ti^{3+} and Ce^{3+}.

B. CO_2 adsorption on Nanocluster modified TiO_2 with oxygen vacancies present

Since oxygen vacancies are stable for our nanocluster-modified TiO_2 composites, we investigate in this section the ability of CO_2 to adsorb at and interact with the oxygen vacancy sites described in the previous section. After forming the oxygen vacancy, we compute the adsorption energies of CO_2 located in different configurations on the reduced nanocluster, with the aim to investigate if there is any transfer of electrons to adsorbed CO_2 and what are the stable adsorption species. We consider the adsorption of CO_2 at the most stable vacancy site of each nanocluster, that is the vacancy with

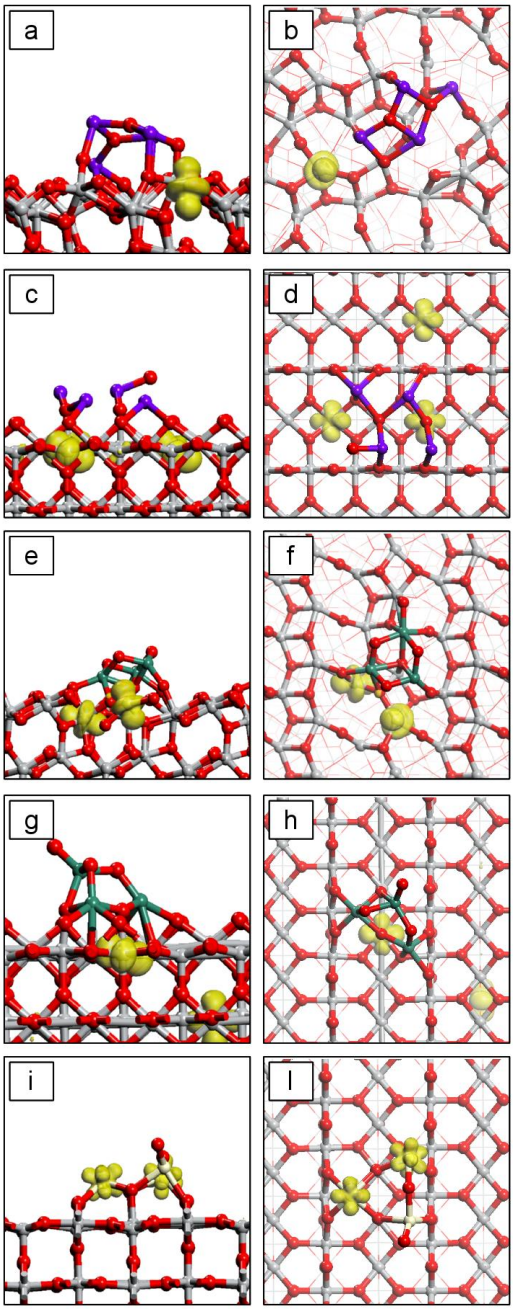


Figure 4: (Color online) Relaxed atomic structure and excess spin-density , where the yellow isosurfaces indicate charge accumulation of Sn_4O_4, Zr_3O_6 and Ce_3O_5 nanocluster modified TiO_2 surfaces after formation of the most stable oxygen vacancy site. a) and b) represent Sn_4O_4 on anatase (101), c) and d) represent Sn_4O_4 on rutile (110), e) and f) represent Zr_3O_6 on anatase (101), g) and h) represent Zr_3O_6 on rutile (110) and i) and l) represent Ce_3O_5 on rutile (110). Light gray and red spheres represent titanium and oxygen atoms, while violet, green and white sphere represent tin, zirconium and cerium atoms, respectively

the lowest formation energy. This will give useful insights in understanding any experimental results that will be obtained for the interaction of CO_2 at these structures; infra-red spectroscopy can be used to determine adsorption structures for the interaction of CO_2 at different TiO_2 structures [56, 57]. The present study focuses on the initial adsorption structures of CO_2, with ongoing work examining

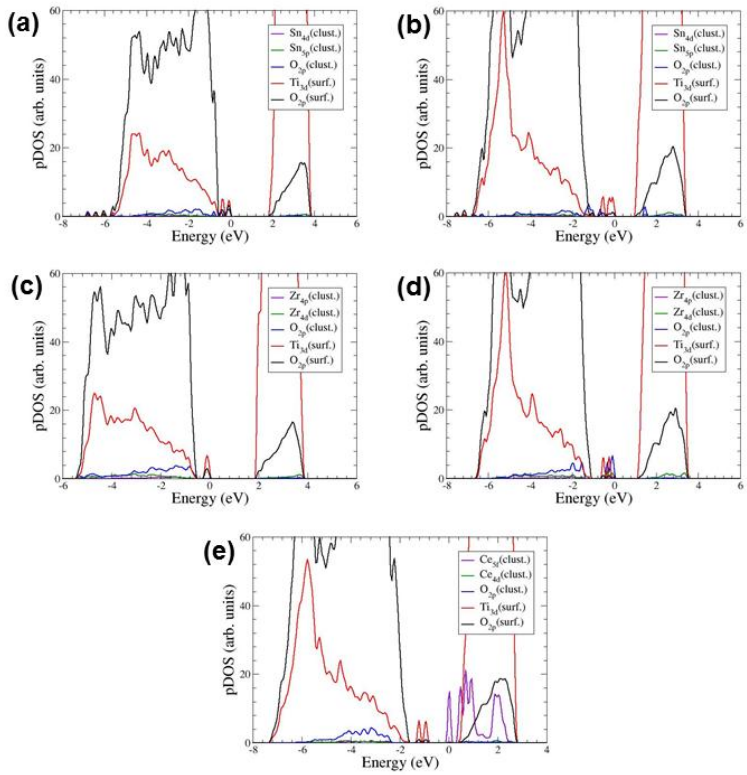


Figure 5: (Color online) Projected electronic density of states for a): Sn_4O_4 modified anatase (101), b) Sn_4O_4 modified rutile (110), c) Zr_3O_6 modified anatase (101), d) Zr_3O_6 modified rutile (110) and e) Ce_3O_5 modified rutile (110) after formation of the most stable oxygen vacancy in each case.

the effect of photoexcitation and interactions with hydrogen to form more complex species.

The adsorption energies of CO_2 have been calculated as described in Eq.1, where CO_2 is the adsorbate. When CO_2 is adsorbed on the reduced Sn_4O_3-anatase (101) surface, we obtain a positive value of the adsorption energy, indicating no adsorption of CO_2. This is most likely a consequence of the very low oxygen vacancy formation energy in this composite, which indicates extremely low reactivity with respect to healing or filling of the oxygen vacancy by oxygen atoms from adsorbed CO_2. We also examined the interaction of CO_2 at the non-reduced Sn_4O_4-anatase composite and here find negative, but small adsorption energies. This indicates some interaction, albeit weak, between CO_2 and this particular composite structure.

For Sn_4O_3-rutile and Ce_3O_4-rutile, the most stable adsorption structures of CO_2 have calculated adsorption energies of -0.32 eV and -0.19 eV, again indicating a weak interaction of CO_2 with these reduced structures. If we adsorb CO_2 at the Ce_3O_5-rutile surface (without the second oxygen vacancy), then the adsorption energy is -0.20 eV.

The most interesting result from the perspective of the adsorption energies is the interaction of CO_2 with the reduced Zr_3O_5-TiO_2 composites, where the computed adsorption energies (in Table III) indicate strong binding of CO_2 to the defective ZrO_2 nanocluster - on anatase, the largest adsorption

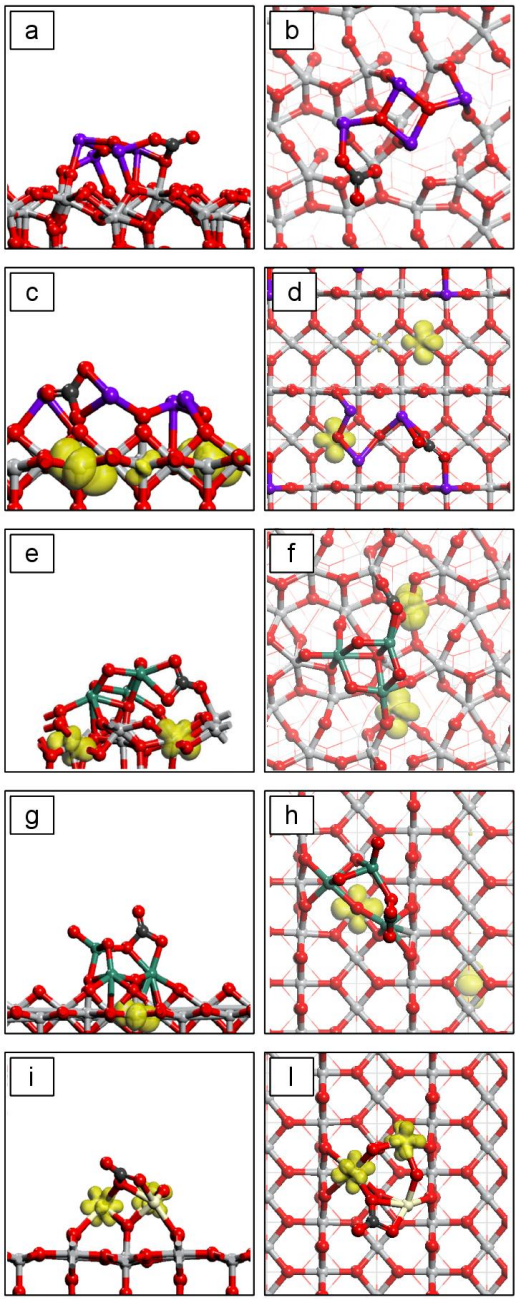


Figure 6: (Color online) Atomic structures after CO_2 adsorption at reduced Sn_4O_3, Zr_3O_5 and Ce_3O_4 nanocluster modified TiO_2 surfaces. a) and b) represent Sn_4O_3 on anatase (101), c) and d) represent Sn_4O_3 on rutile (110), e) and f) represent Zr_3O_5 on anatase (101), g) and h) represent Zr_3O_5 on rutile (110) and i) and l) represent Ce_3O_4 on rutile (110). Light gray and red spheres represent titanium and oxygen atoms, while violet, green and white and dark gray sphere represent tin, zirconium, cerium and carbon atoms, respectively

energy is -1.21 eV, while on rutile it is -0.94 eV.

Thus, the strength of the interaction between CO_2 and the supported metal oxide nanoclusters we have considered in this paper depends rather strongly on the identity of the supported metal oxide nanocluster and its reducibility. The most reducible nanoclusters, Sn_4O_4 and Ce_3O_5, with very small oxygen vacancy formation energies show rather weak interactions with CO_2 and in fact there is little

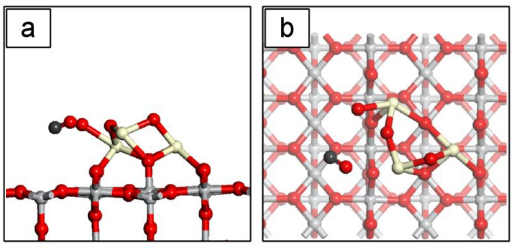


Figure 7: (Color online) Atomic structure for CO formation after CO_2 adsorption on Ce_3O_5-V_O rutile (110)TiO_2. Light gray and red spheres represent titanium and oxygen atoms, while white and dark gray sphere represent cerium and carbon atoms, respectively

difference between the interaction of CO_2 with the perfect or defective supported nanoclusters. By contrast, on a reduced supported ZrO_2 nanocluster, the interaction with CO_2 is much stronger. We attribute this difference to the balance between oxygen vacancy formation and vacancy healing (or filling) - by lowering the cost to form an oxygen vacancy, it then becomes more difficult to fill the vacancy using oxygen from a source such as CO_2 (in addition to the high stability of CO_2). Conversely, if the cost to form the oxygen vacancy is larger, then filling of the vacancy becomes more favourable. It therefore appears that from this perspective, ZrO_2 modified rutile or anatase will interact with CO_2.

DFT and experimental studies of the interaction of CO_2 with extended surfaces of ZrO_2, SnO and CeO_2 have been published in refs [58–63] For ZrO_2 Hornebecq et al [58] found weak adsorption energies of 0.2 to 0.3 eV and the case of stronger adsorption energies of 0.7 eV corresponded to the interaction with structural defects, which would be consistent with our finding of strong CO_2 adsorption at defective ZrO_2. Bachiller-Baeza et al [59] show that CO_2 forms carbonates on ZrO_2 and that the stability of CO_2 depends on the crystal form of ZrO_2; treating the sample under reducing conditions gave adsorption energies from calorimetry in the range of 1 to 1.39 eV. Allowing O_2 treatment prevented this particularly strong adsorption process so that it was proposed that formation of oxygen vacancies facilitated the interaction with CO_2.

There are no literature reports of the interaction of CO_2 with SnO; in fact there are few reports on the interaction of CO_2 with any tin oxides. In Refs. [60, 61], the interaction of CO_2 is weak and the adsorbed species are carbonates with different adsorption modes.

On ceria surfaces, Cheng et al [62] studied adsorption of CO_2 at oxidised and reduced CeO_2 (110) with DFT+U. Adsorption was most favourable on the reduced surface to form a monodentate carbonate species, with an adsorption energy of 1.23 eV and transfer of an electron from a Ce^{3+} cation to CO_2. On the CeO_2 (111) surface, Reimers et al [63] found that adsorption at the reduced (111) surface is stronger than at the oxidised surface, with adsoprtion energes of 0.91 eV

and 0.37 eV, respectively. A carbonate is present on the oxidised (111) surface. The difference between the results on the extended surfaces and the supported ceria nanocluster arises from the very low cost to form the oxygen vacancy in the ceria nanocluster which makes filling of the vacancy difficult.

Table III: Computed adsorption energies, in eV, of CO_2 on Sn_4O_3, Zr_3O_5 and Ce_3O_4 nanocluster modified anatase (101) and rutile (110) TiO_2 surfaces.

Nanocluster-TiO_2 Structure	Adsorption Energy (eV)
Anatase (101)-Sn_4O_4-CO_2-I	−0.21
Anatase (101)-Sn_4O_4-CO_2-II	−0.12
Anatase (101)-Sn_4O_4-CO_2-III	−0.15
Anatase (101)-Sn_4O_4-V_O-CO_2-I	0.07
Rutile (101)-Sn_4O_4-V_O-CO_2-I	−0.32
Anatase (101)-Zr_3O_6-V_O-CO_2-I	−1.21
Anatase (101)-Zr_3O_6-V_O-CO_2-II	−1.08
Anatase (101)-Zr_3O_6-V_O-CO_2-III	−0.53
Anatase (101)-Zr_3O_6-V_O-CO_2-IV	−0.21
Rutile (101)-Zr_3O_6-V_O-CO_2-I	−0.94
Rutile (101)-Zr_3O_6-V_O-CO_2-II	−0.62
Rutile (101)-Ce_3O_5-V_O-CO_2-I	−0.11
Rutile (101)-Ce_3O_5-V_O-CO_2-II	−0.19
Rutile (101)-Ce_3O_5-V_O-CO_2-III	0.12
Rutile (101)-Ce_3O_5-CO_2-I	−0.20
Rutile (101)-Ce_3O_5-CO	−0.29

We next discuss the structure of adsorbed CO_2 on nanocluster modified TiO_2, with the atomic structure of the most stable adsorption structures shown in figure 6, along with the corresponding excess spin density. The analysis of the geometry shows that after CO_2 adsorption and relaxation, the most stable adsorption structure tends to be a CO_3-like complex that is formed upon the interaction of adsorbed CO_2, with lattice oxygen from the supported nanoclusters. The adsorption of CO_2 at the oxygen vacancy site results in the displacement of an oxygen atom in the nanocluster to make a new C-O bond leading to the formation of a surface bound carbonate species. Furthermore, the carbonate is also adsorbed in a bidentate form, that is with two oxygen atoms bound to cations in the nanocluster or the surface. Examining the adsorption structures in more detail, we see that there are two possible bidentate carbonate adsorption configurations: the first is the “bridging”, where the carbonate forms bonds with cations in the NC and the surface, and “top”, where the carbonate only

forms bonds with cations in the NC.

We found the most stable adsorption configurations of CO_2 to be the "bridge" for Sn_4O_4-anatase (101) and Sn_4O_3-rutile (110) and for Zr_3O_5-anatase (101). The "top" adsorption configuration is found for adsorption on Zr_3O_5-rutile (110) and Ce_3O_4-rutile (110). This configuration has Zr and Ce cations in a chelating-like bidentate bonding configuration. The O-C-O angles and C-O lengths are comparable to the carbonate moiety, with small distortions of the O-C-O angles due to the reduced symmetry in the CO_2-NC adsorption structure. Typical C-O bond lengths are 1.21 Å for the terminal oxygen (that does not bind to the surface) and 1.32 and 1.41 Å for the oxygen that make the bidentate bonds to the oxide nanoclusters.

There is another interesting scenario in which we find spontaneous formation of free CO upon breaking of a C-O bond in CO_2 upon adsorption on the Ce_3O_4-rutile composite. The interaction with CO_2 results in the healing of the oxygen vacancy site, forming Ce_3O_5, and there is a small energy gain of -0.29 eV. These energetics for CO_2 adsorption at a reduced Ce_3O_4-rutile composite suggest that adsorbed carbonate species and free CO can both be present.

After CO_2 adsorption, the excess spin-density suggests no differences in the distribution of reduced cations when compared with the reduced nanocluster modified surfaces: when the carbonate forms, there are two reduced Ti^{3+} cations in the rutile and anatase surfaces and reduced Ce^{3+} cations in the reduced Ce_3O_4 nanocluster.

IV. DISCUSSION

The results presented in this paper build on our previous work in developing new photocatalysts where we focussed on the band gap change and charge separation in surface modified TiO_2. To use these composite materials in the CO_2 reduction process now requires examination of their reduction through formation of oxygen vacancies and the subsequent interaction with CO_2 to investigate if CO_2 can be activated by these structures. The latter is obviously a key step in CO_2 reduction using photocatalysis.

For the potential red shift in light absorption and charge separation, the simple projected density of states plots in figure 2 show that the nanocluster modification of rutile and anatase will indeed induce a red shift in light absorption. The composition of the valence and conduction bands in the composite structure indicates favourable charge separation, with hole localisation on the nanocluster and electron localisation on the TiO_2 surface [30–32, 47, 48]. Thus two key requirements for a photocatalyst are met in these structures.

The energy cost to form an oxygen vacancy in SnO- and CeO_2-modified rutile and anatase is small

and these nanoclusters would be non-stoichiometric under typical experimental conditions. There is a larger energy cost to form an oxygen vacancy in ZrO_2-modified rutile and anatase which is still small enough to be considered favourable for reduction.

The interaction with CO_2 at the vacancy site can heal the oxygen vacancy, giving a free CO and oxygen that fills the vacancy site or adsorption and electron transfer to CO_2 to activate it or formation of surface bound carbonate species. For the interaction of CO_2 with reduced SnO and CeO_2 nanoclusters, the CO_2 molecule interacts rather weakly at the reduced nanocluster forming carbonate-like adsorbates; while these can be identified through infra-red spectroscopy they may not be the preferred adsorption species for activating CO_2. Interestingly, in the case of reduced ZrO_2 nanoclusters, the adsorption of CO_2 to form a bidentate carbonate bound at the surface is favourable. We attribute this difference to the reducibility of the nanocluster modifier: the very low formation energy of oxygen vacancies in SnO and CeO_2 modified TiO_2 means that filling the vacancy site with CO_2 is not favourable. Conversely, the higher cost to form an oxygen vacancy in ZrO_2 means the reduced nanocluster will interact more strongly with CO_2.

We find an interesting result for the reduced CeO_2 nanocluster, where the adsorption of CO_2 can result in breaking of a C-O bond and formation of free CO. This indicates the possibility to activate CO_2 using CeO_2 as a TiO_2 modifier; such a composite has been studied for water gas shift by Rodriguez and co-workers [46, 64] where it facilitates the dissociation of water when compared with extended ceria surfaces or unmodified TiO_2.

This is the first study of metal oxide nanocluster modified TiO_2 composites, for which visible light activity is predicted, to focus on the reducibility and their interaction with CO_2 to probe the potential for these new materials to activate CO_2. There are some useful general points that can be made with regard to CO_2 activation that will be of interest in this field:

(1) The reducibility of the nanocluster modifier (and the composite as a whole) is important - if it is too easily reduced then the interaction with CO_2 will be potentially too weak to activate the CO_2. Thus, we seek systems that can be reduced without requiring high temperatures but are not so easily reduced that this process occurs at very low temperature.

(2) Nanoclusters offering low coordinated metal sites can provide sites for CO_2 to adsorb.

(3) The presence of reducible cations in the nanocluster, e.g. CeO_2, may also facilitate CO_2 activation.

(4) The calculations presented herein focussed on thermal processes - reduction of nanocluster-modified TiO_2 and interaction with CO_2. However, given that these novel photocatalyst structures can be excited with visible light, this allows a combined photo- and thermal-catalytic approach to activating CO_2 with electrons provided from reduced cations (thermal vacancy formation) and photoexcitation. This forms the basis of future work on CO_2 activation on composite structures that display an ability

to activate CO_2.

(5) The conduction band potential of a photocatalyst material relative to CO_2 reduction is also important as we aim to excite the photocatalyst and use the excited electron to activate CO_2. Unfortunately, the position of the TiO_2 conduction band is not suitable for this process. While there are other semiconductor photocatalysts such as SiC or phosophides that show suitable conduction band potentials, these materials suffer from other issues. There is at present, no single photocatalyst that can successfully activate CO_2 to make useful fuels [7, 10]

However, the last two points are the subject of ongoing work to examine the effect of photoexcitation on CO_2 activation on surface modified TiO_2.

V. CONCLUSION

We have presented a DFT level study of the interaction of CO_2 with metal oxide nanocluster modified TiO_2 surfaces. We calculated the oxygen vacancy formation energies for Sn_4O_4, Zr_3O_6 nanoclusters on TiO_2 anatase (110) and rutile (110), and Ce_3O_5 nanocluater on rutile (110) surfaces, and we examined CO_2 adsorption at the most stable vacancy sites. We found the formation of carbonate group on each structure with one oxygen of the CO_2 healing the nanocluster vacancy, with the exception of the Sn_4O_4 on anatase (101) where CO_2 adsorbs only on the stoichiometric NC, and interestingly, we found a spontaneous formation of CO after CO_2 adsorption on Ce_3O_5-rutile (110) surface. The main results in the present paper do show that carbonates can be formed upon interaction of metal oxide nanocluster modified TiO_2 with CO_2 and that it is also possible to break a C-O bond to form free CO, demonstrating the great potential of these novel composite materials for CO_2 activation.

VI. ACKNOWLEDGEMENTS

We acknowledge support from Science Foundation Ireland (SFI) through the US-Ireland R&D Partnership Program, grant number SFI 14/US/E2915 and the European Commission through the COST Action CM1104 “Reducible Metal Oxides, Structure and Function”. We acknowledge access to computing resources at Tyndall provided by SFI and by the SFI and Higher Education Authority funded Irish Centre for High End Computing. We acknowledge discussions with Profs. Kimberly Gray and Eric Weitz.

[1] K. Kermeli, W. H. J. Graus, and E. Worral. *Energy Effic.*, page 987, 2014.

[2] G. Pleßmann, M Erdmann, M. Hlusiak, and Ch. Breyer. *8th Int. Renew. Energy Storage Conf. Exhib.*, page 1, 2013.

[3] M. Pelaez, N. T. Nolan, J. A. Byrne, S. C. Pillai, M. K. Seery, P. Falaras, A. G. Kontos, P. S. M. Dunlop, J. W. J. Hamilton, K. O'Shea J. A. Byrne, M. H. Entezari, and D. D. Dionysiou. *Appl. Cat. B.*, 125:331, 2012.

[4] S. C. Pillai, U. L. Stanger, J. A. Byrne, A. Perez-Larios, and D. D. Dionysiou. *Chem. Eng. J.*, 261:1, 2015.

[5] V. Etacheri, C. Di Valentin, J. Schneider, D. Bahnemann, and S. C. Pillai. *J. Photochem. and Photobiol. C: Photochemistry Reviews*, 25:1, 2015.

[6] A. Kubacka, M. Fernandez-Garcia, and G. Colon. *Chem. Rev.*, 112:1555, 2012.

[7] S. Roy, O. K. Varghese, M. Paulose, and C. A. Grimes. *ACS Nano*, 4:1259, 2010.

[8] W. Kim, T. Seok, and W. Choi. *Energy and Environmental Science*, 5:6066, 2012.

[9] N. M. Dimitrijevic, I. A. Shkrob, D. Gosztola, and T. Rajh. *J. Phys. Chem C.*, 116:878, 2012.

[10] L. Schmidt-Mende, J. K. Stolarczyk, and S. N. Habisreutinger. *Angew. Chem.*, 52:7372, 2013.

[11] U. Diebold. *Appl. Phys. A Mater. Sci. Process.*, 76:681, 2003.

[12] A. Fuerte, M. D. Hernandez-Alonso, A. J. Maira, A. Martinez-Arias, M. Fernandez-Garcia, J. C. Conesa, and J. Soria. *Chem. Commun.*, page 2718, 2001.

[13] W. Li. *Phys. status solidi - Rapid Res. Lett.*, 9:10, 2015.

[14] M. Anpo. *Pure Appl. Chem.*, 72:1787, 2000.

[15] K. Ozawa, M. Emori, S. Yamamoto, R. Yukawa, S. Yamamoto, R. Hobara, K. Fujikawa, H. Sakama, and I. Matsuda. *J. Phys. Chem. Lett.*, 5:1953, 2014.

[16] K. Woan, G. Pyrgiotakis, and W. Sigmund. *Adv. Mater.*, 21:2233, 2009.

[17] N. T. Nolan, M. K. Seery, and S. C. Pillai. *J. Phys. Chem. C*, 113:16151, 2009.

[18] N. T. Nolan, M. K. Seery, S. J. Hinder, L. F. Healy, and S. C. Pillai. *J. Phys. Chem. C*, 114:13026, 2010.

[19] X. L. Nie, S. P. Zhou, G. Maeng, and K. Sohlberg. *Int. J. Photoenergy*, page 294042.

[20] D. Wei. *Int. J. Mol. Sci.*, 11:1103, 2010.

[21] M. Gratzel. *J. Photochem. and Photobiol. C*, 4:145, 2003.

[22] M. Gratzel. *Acc. Chem. Res.*, 42:1788, 2009.

[23] H. Tada, T. Mitsui, T. Kiyonaga1, T. Akita, and K. Tanaka. *Nature Mat.*, 5:782, 2006.

[24] M. Fujii, K. Nagasuna, M. Fujishima, T. Akita, and H. Tada. *J. Phys. Chem. C*, 113:16711, 2009.

[25] T. Kiyonaga, T. Akita, and H. Tada. *Chem. Commun.*, page 2011, 2009.

[26] C. Sahoo and A. K. Gupta. *J. Environ. Sci. Health. A. Tox. Hazard. Subst. Environ. Eng.*, 50:659, 2015.

[27] J. Liu, Q. Zhang, J. Yang, H. Ma, M. O. Tade, S. Wang, and J. Liu. *Chem. Commun.*, 50:13971, 2014.

[28] H. Tada, Q. Jin, H. Nishijima, H. Yamamoto, M. Fujishima, S. Okuoka, T. Hattori, Y. Sumida, and H. Kobayashi. *Angew. Chem. Int. Ed. Engl.*, 50:3501, 2011.

[29] H. Tada, Q. Jin, A. Iwaszuk, and M. Nolan. *J. Phys. Chem. C*, 118:12077, 2014.

[30] M. Nolan, A. Iwaszuk, and K. A. Gray. *J. Phys. Chem. C*, 118:27890, 2014.

[31] A. Iwaszuk, A. K. Lucid, K. M. Razeeb, and M. Nolan. *J. Mat. Chem. A*, 2:18796, 2014.

[32] M. Nolan. *ACS Appl. Mater. Interfaces*, 4:5863, 2012.

[33] A. Iwaszuk, M. Nolan, Q. Jin, M. Fujishima, and H. Tada. *J. Phys. Chem. C*, 117:2709, 2013.

[34] M. Fujishima, Q. Jin, H. Yamamoto, H. Tada, and M. Nolan. *Chem. Phys. Phys. Chem.*, 14:705, 2012.

[35] Q. Jin, M. Fujishima, M. Nolan, A. Iwaszuk, and H. Tada. *J. Phys. Chem. C*, 116:12621, 2012.

[36] Q. Jin, M. Fujishima, A. Iwaszuk, M. Nolan, and H. Tada. *J. Phys. Chem. C*, 117:23848, 2013.

[37] H. Shi, Y. Liu, Z. Zhao, M. Miao, T. Wu, and Q. Wang. *J. Phys. Chem. C*, 118:20257, 2014.

[38] A. Albuquerque, A. Bruix, J. R Sambrano, and F. Illas. *J. Phys. Chem. C*, 119:4805, 2015.

[39] J. P. Perdew, K. Burke, and M. Ernzerhof. *Phys. Rev. Lett.*, 77:3865, 1996.

[40] G. Kresse and J. Furthmuller. *Comput. Mater. Sci.*, 6:15, 1996.

[41] G. Kresse and J. Furthmuller. *Phys. Rev B*, 15:11169, 1996.

[42] P. E. Blocl. *Phys. Rev. B*, 50:17953, 1994.

[43] M. Nolan, S. C. Parker, and G. W. Watson. *Surf. Sci.*, 595:223, 2005.

[44] M. Nolan. *J. Phys. Chem. C*, 115:6671, 2011.

[45] A. Iwaszuk and M. Nolan. *J. Phys.: Cond. Matt.*, 23:334207, 2011.

[46] J. Graciani, J. J. Plata, J. Fdez. Sanz, P. Liu, and J. A. Rodriguez. *J. Chem. Phys.*, 132:104703, 2010.

[47] A. Iwaszuk, P. A. Mulheran, and M. Nolan. *J. Mater. Chem. A*, 1:2515, 2013.

[48] A. Iwaszuk and M. Nolan. *Phys. Chem. Chem. Phys.*, 13:4963, 2011.

[49] A. Iwaszuk M. and Nolan. *J. Mater. Chem. A*, 1:6670, 2013.

[50] A. Iwaszuk and M. Nolan. *Catal. Sci. Technol.*, 3:2000, 2013.

[51] M. Nolan. *in Catalysis by Materials with Well-Defined Structures.* Eds. S. Overbury and Z. Wu, Elsevier, 2015.

[52] A. Togo, F. Oba, I. Tanaka, and K. Tatsumi. *Phys. Rev. B*, 74:195128, 2006.

[53] A. S. Foster, V. B. Sulimov, F. Lopez Gejo, A. L. Shluger, and R. M. Nieminen. *Phys. Rev. B*, 64:224108, 2001.

[54] M. Nolan, J. E. Fearon, and G. W. Watson. *Solid State Ionics*, 177:3069, 2006.

[55] S. Fabris, G. Vicario, G. Balducci, S. De Gironcoli, and S. Baroni. *J. Phys. Chem. B*, 109:22860, 2005.

[56] K. Bhattacharyya, W. Wu, E. Weitz, B. Vijayan, and K. A. Gray. *Molecules*, 20:15469, 2015.

[57] W. Wu, K. Bhattacharyya, K. A. Gray, and E. Weitz. *J. Phys. Chem. C*, 117:20643, 2013.

[58] V. Hornebecq, C. Knofel, P. Boulet, B. Kuchta, and P. L. Llewellyn. *J. Phys. Chem. C*, 115:10097, 2011.

[59] B. Bachiller-Baeza, I. Rodriguez-Ramos, and A. Guerrero-Ruiz. *Langmuir*, 14:3556, 1998.

[60] E. W. Thornton and P.G. Harrison. *J. Chem. Soc. Faraday Trans.*, 1:461, 1975.

[61] M. Melle-Franco, G. Pacchioni, and A.V. Chadwick. *Surf. Sci.*, 478:25, 2001.

[62] Z. Cheng, B. J. Sherman, and C. S. Lo. *J. Chem. Phys.*, 138:014702, 2013.

[63] W. G. Reimers, M. A. Baltanas, and M. M. Branda. *J. Mol. Model.*, 20:2270, 2014.

[64] J. B. Park, J. Graciani, J. Evans, D. Stacchiola, S. Ma, P. Liu, A. Nambu, J. Fernandez Sanz, J. Hrbek, and J. A. Rodriguez. *Proc. Natl. Acad. Sci.*, 106:4975, 2009.